4-2016

Large-area Object Search and Recovery using Sector-based Aerial Acousto-optic Scanning and Reflection Sensing

Monish Ranjan Chatterjee
University of Dayton, mchatterjee1@udayton.edu

Salaheddeen G. Bugoffa
University of Dayton

Large-area object search and recovery using sector-based aerial acousto-optic scanning and reflection sensing

Monish R. Chatterjee[1,*] and Salaheddeen G. Bugoffa[1]

[1]Department of Electrical & Computer Engineering

University of Dayton, Dayton, Ohio 45469

[*]Corresponding author

Email: mchatterjee1@udayton.edu; Tel.: (937) 229 3594

ABSTRACT

A sector-based angular scanning system intended to identify and spatially locate relatively small objects scattered over a large terrain is described in this paper. The system is modeled as a planar surface on the horizontal (XY) plane, with an acousto-optic Bragg cell on board an unmanned aerial vehicle (UAV) operating in the XZ plane. The Bragg cell is excited by a chirped RF signal with a designed frequency ramp. As the scanning beam reflects off the horizontal surface, a detector placed strategically at a suitable altitude (in the analysis shown to be on board the UAV itself) picks up the reflected wave and thereafter evaluates the refractive index of the material at the location using the Fresnel reflection coefficient. For large area coverage, the UAV makes alternate 180-degree turns at the end of each row-scan, thereby after several row scans, a practical surface area is covered. The usefulness and limitations of this scanning method are discussed.

Keywords: acousto-optics, beam steering, Gaussian beam, sector-based laser scanning, Bragg cell, Fresnel coefficients, UAV

1. INTRODUCTION

Acousto-optic beam steering has been used over the years for a variety of applications [1, 2]. The ability to steer laser beams at high frequencies (tens of MHz to a few GHz) electronically with high angular resolution (given Bragg angles in the mrad range) makes the Bragg cell an ideal device for angular and spatial steering. In this paper, we describe a simple sector-based angular scanning system intended to cover a large surface area in order to identify and spatially locate relatively small objects scattered over the terrain [3]. The scanning system is modeled as a planar surface on the horizontal (XY) plane, with an acousto-optic Bragg cell (on board a UAV) operating in the XZ plane. The Bragg cell is excited by a chirped RF signal with frequency ramping from low-to-high or high-to-low. As the scanning beam reflects off the horizontal surface, a detector placed on the UAV picks up the reflected wave (shown to be effective over the scan range), and thereby evaluates the refractive index of the material at the location on the basis of the corresponding Fresnel reflection coefficient [4]. If the surface, say, is primarily sea water, then the detection is considered "negative" unless a material different from sea water is detected. Following each horizontal scan (about 374.15 m), the return path is a blank. The Bragg cell, mounted on a stepper motor, is then rotated in the horizontal plane by a small angle, and the second scan run is carried out from the rotated position. Following this process with only L-to-R or R-to-L active scans and interleaving blanks, a "unit" circular sector is scanned with physical dimensions approximately 374.15 m × 300 m. Any "positive" refractive index returned by the sensor is stored in the system in terms of the spatial coordinates of the scanned point. Since the unit sector does not entirely cover a rectangular area or grid, the coverage efficiency can be increased by rotating the Bragg cell from its nominal XZ plane by approximately 90^0 such that it then moves to the YZ plane. Under this configuration, another series of horizontal scans in the XY is carried out, providing additional scanning area that includes portions of the grid previously left out. In reality (as will be discussed below) the actual rotation angle is chosen to be 107^0 which allows the scan coverage to be maximal. In this manner, incidentally, some portions of the unit grid may be scanned more than once. This would lead to possible "positive" detection of objects multiple times. The scanning scheme

Signal Processing, Sensor/Information Fusion, and Target Recognition XXV, edited by Ivan Kadar, Proc. of SPIE Vol. 9842, 98421C · © 2016 SPIE · CCC code: 0277-786X/16/$18 · doi: 10.1117/12.2229024

consists of a horizontal row (along Z) reached via multiple grid scans along the Z axis until a chosen scanning distance (about 30 km in this design) is reached, following which the UAV is instructed to reverse direction of flight, and a new row scan is carried out in the reverse direction along an incremental change in Y along the horizontal plane. In this manner, a series of horizontal scans covering an arbitrarily large surface area is carried out (technically over a few hundred square km or the equivalent of a moderate-sized city). The scheme is shown in the numerical simulation to yield coordinate locations of any arbitrary distribution of non-sea-water materials randomly scattered over the scanned surface. This scanning system may be useful in search and rescue applications over large surface areas (especially is unreachable terrains directly below the UAV) using the A-O scanning methodology via a Bragg cell mounted on board at an altitude of approximately 8 km.

The paper is organized as follows. Section 2 presents an overview of A-O scanning by using frequency chirps. A schematic 2D-scanning configuration based on A-O scanning and aerial transportation provided by a UAV is described in section 3. Numerical analysis of 2D- scanning scheme is reported in some detail in section 4. Simulation results and their limitation are outlined in section 5. Section 6 presents concluding remarks and ideas to further expand the research for more complex terrains.

2. A-O SCANNING USING FREQUENCY CHIRP

Acousto-optics involves interaction between sound and light that used in many applications, including electronic control of the intensity and positioning of a laser beam. When an incident laser beam passes through a Bragg cell it diffract into many orders. In the so-called Bragg regime of operation, the incident beam is scattered into two orders (zeroth and first). The diffraction efficiency (η_D) is defined as the ratio of the first-order scattered intensity relative to the incident intensity, and in the perfect Bragg case, is given by:

$$\eta_D = \sin^2 \frac{\alpha_0 \xi}{2},$$

where α_0 is the so-called effective phase delay of the light passing through the sound column, and ξ (= z/L with L being the interaction length within the Bragg cell) is the normalized distance of propagation with the sound cell [5, 6].

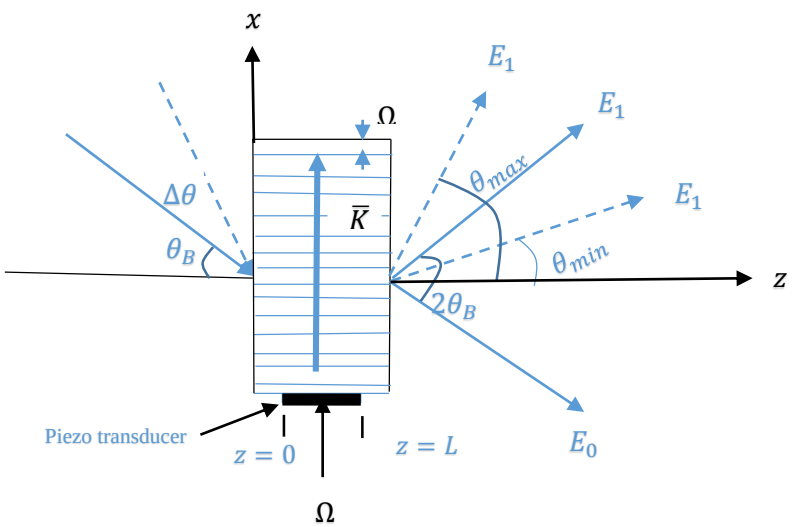

Fig.1. Schematic representation of Bragg cell showing input and output deviations.

As can be seen in Fig.1, an A-O Bragg cell with perfect Bragg incidence ($\theta_{inc} = \theta_B$) produces two scattered orders, zeroth- and first-order, shown by solid lines. It turns out that the effective Bragg angle changes in direct proportion to the RF (sound) frequency (Ω); hence, by changing Ω, the direction of the first-order scattered beam may also be altered. It is this feature that makes it possible to use an acousto-optic modulator as a laser beam deflector and scanner [7]. While changing Ω changes the direction of the scattered light, it must be noted that unless the incident angle is adjusted to the

new Bragg angle (a Bragg mismatch), the overall scattering efficiency will likely decrease. Hence, the operation of an A-O scanner must take the overall loss of efficiency into account if the incident beam is fixed at a specific angle. Moreover. If the Bragg angle changes drastically, the device may no longer operate in the Bragg regime. In such a case, there may likely be higher scattered orders, thereby potentially making the first order even less efficient. In the current application, the RF frequency (Ω) is varied between 350 MHZ to 1050 MHZ, thereby yielding a minimum Bragg angle of $\theta_{B,min} = 0.02334$ rad and a maximum Bragg angle of $\theta_{B,max} = 0.07$ rad, assuming the sound velocity v_s to be 3 km/s. As will be shown, these angles directly translate in the scanning system to the minimum and maximum scan angles of incidence on the surface to be scanned. Additionally, it will be shown that for the entire range of RF frequencies, the Q (to be defined later) of the device remains sufficiently high to ensure Bragg operation. These angles represent the limits of the scanning beam over a spatial distance (d_s) in the horizontal (XY) plane shown to be approximately 374.15 m [8], as depicted in Fig.2.

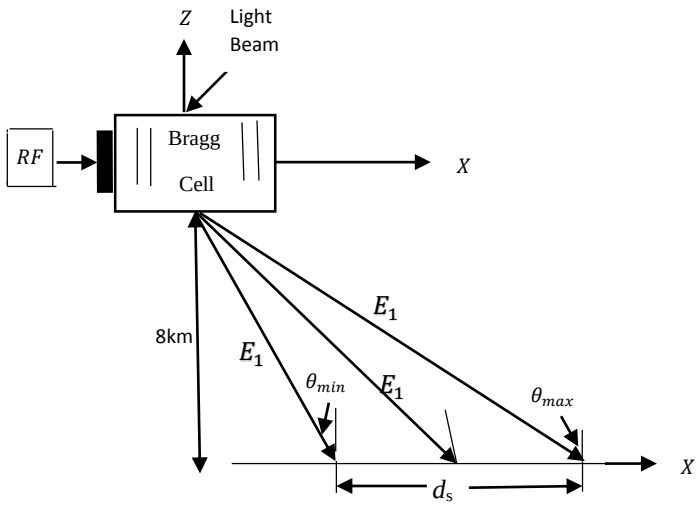

Fig.2. Bragg layout and relative orientation of first-order Bragg diffraction with minimum and maximum incident angle and scanning distance

Since the Q (Klein-Cook) parameter is given by:

$$Q = \frac{4\pi L}{n v_s}(\Omega\theta_B) \quad , \tag{1}$$

where, L is the interaction length, n is the index of refraction of the dielectric, v_s is the sound velocity, Ω is the sound frequency, and θ_B is the Bragg angle. Chatterjee and Chen have showed that for strict Bragg operation, Q needs to be greater than 8π [9]. In order to make this condition ($Q \gg 8\pi$) valid, the length of the Bragg cell is chosen to be 10cm. It is clear from eq. (1), since Q is proportional $\Omega\theta_B$, and the values of Q within the chosen Ω-range are found as $Q_{center} = 9100$, $Q_{\min} = 2274$, $Q_{\max} = 20460$. The reason Q increases nonlinearly with Ω is because θ_B is also proportional to Ω, thereby effectively making Q vary as Ω^2. Hence the Qs satisfy the Bragg condition.

2.1 Photodetector sensitivity considerations

The photodetector must be designed so that it is sensitive enough to capture the incident light even after it has undergone loss of power due to (i) the Bragg cell efficiency, and (ii) the power reflection coefficient from the reflection on the ground

across the scanning distance. Accordingly, we begin by considering the Bragg cell scattering efficiency under non-ideal conditions due to deviations from the actual Bragg angle when the RF frequency changes and the incident light beam is fixed at the Bragg angle for the center RF frequency (700 MHz). The first-order efficiency is given by [10]

$$\eta_D = \frac{(\frac{\hat{\alpha}_0}{2})^2}{(\frac{\delta Q}{4})^2+(\frac{\alpha_0}{2})^2} * \ sin^2(\sqrt{(\frac{\delta Q}{4})^2 + (\frac{\alpha_0}{2})^2}) \quad \text{, where} \tag{2}$$

η diffraction efficiency,

$\hat{\alpha}_0$ peak phase delay, and

Q Klein-Cook parameter.

Based on the parameters chosen, the Bragg angle deviation is found to be $\delta = \frac{\Delta\Omega}{\Omega_{center}} = \pm 0.5$; the peak phase delay is chosen to be $\hat{\alpha}_0 = 51\pi$, the efficiency is found to be $\eta_D = 100\%$ at center frequency (700 MHZ), $\eta_D = 3.7900\%$ at the maximum frequency (1050 MHZ), and $\eta_D = 0.0040\ \%$ at the minimum frequency (350 MHZ). The choice of $\hat{\alpha}_0$ above needs some further explanation. We note from eq.(2) that since Q for this problem is fairly high, the efficiency of the Bragg cell would be very low unless one chooses to operate the cell at sufficiently high $\hat{\alpha}_0$. We note also that the chosen $\hat{\alpha}_0$ has to be an odd multiple of π, such that even under zero deviation, we obtain the maximum value of the sine term in eq.(2). Technically, one could pick an arbitrarily large (odd) value of $\hat{\alpha}_0$; however, we note that $\hat{\alpha}_0$ depends directly on the applied RF or acoustic power from the sound cell driver. Hence, there is a physical limit to the value of $\hat{\alpha}_0$ that is permissible under the RF power limitations of the source. We note that even with this choice of $\hat{\alpha}_0$, the efficiencies achieved are still rather low (from about 2% to about 20%). From this perspective, it appears that the value 51π may place the required source power in the permissible range. Next, we note that under reflection from a planar surface with perpendicularly polarized light (whose rationale explain below), the power reflection coefficient is given by

$$\frac{s^{ref}{}_{avg}}{s^{i}{}_{avg}} = |\Gamma_\perp|^2 \ , \tag{3}$$

where $\Gamma_\perp$ is the Fresnel amplitude reflection coefficient for perpendicular polarization.

Note that the Fresnel amplitude reflection coefficient for perpendicular polarization is given by:

$$\Gamma_\perp = \frac{\eta_2 \cos\theta_i - \eta_1 \cos\theta_t}{\eta_2 \cos\theta_i + \eta_1 \cos\theta_t} \ , \tag{4}$$

where η_1 and η_2 are the wave impedances ($= \sqrt{\frac{\mu_{1,2}}{\varepsilon_{1,2}}}$) in the two media, expressible in terms of their permittivities and permeabilities; also, θ_i and θ_t are the angles of incidence and transmission respectively. For *nonmagnetic* ($\mu_r = 1$) media, the above equations reduce to:

$$\Gamma_\perp = \frac{n_1 \cos\theta_i - n_2 \cos\theta_t}{n_1 \cos\theta_i + n_2 \cos\theta_t} \ , \tag{5}$$

where n_1 and n_2 are the (phase) refractive indices of the two media. Also, $\Gamma_\perp$ is calculated by invoking Snell's law generalized as follows:

$$\beta_1 \sin\theta_i = \beta_2 \sin\theta_t \quad , \tag{6}$$

where β_1 and β_2 are the unbounded wavenumbers $(= \omega\sqrt{\mu_{1,2}\,\varepsilon_{1,2}})$ in the two media where ω is the radian optical frequency.

The reason for choosing perpendicularly polarized light for the scanning problem is to avoid any possible Brewster condition during the reflection from the scanned surface, since the detection of the reflecting material is based on measuring the reflected light.

With the above two conditions, one obtains the power incident at the photodetector as:

$$P_D = P_{inc}\,\eta_D\,|\Gamma_\perp|^2 = P_{inc}\,p \quad , \tag{7}$$

where p is a figure of merit.

Based on the above, with an incident laser power at the input of the Bragg cell being, say, 25 mW, the resulting reflected power reaching the photodetector may be readily calculated. This number, of course, will change due to the change of the RF frequency, and also the incident angle at the interface which is the same as the corresponding Bragg angle of operation. This in turn changes the Fresnel power coefficient. We note at this stage that the reflected power in this problem varies nonlinearly with the product $\eta_D\,|\Gamma_\perp|^2$. Table 1 shows in detail the Bragg angles, Fresnel coefficients, diffraction efficiencies, the figure of merit p, and the photodetector power for the case of plastic as an example. Similar tables are needed in order to establish the range of possible photodetector power levels across a range of chosen nonmagnetic materials [Bugoffa thesis].

Table1. Reflected power from air-plastic interface incident at the photodetector

Ω	$\theta_B = \theta_i$	η_D	$\Gamma_\perp$	$p = \eta_D\,\lvert\Gamma_\perp\rvert^2$	p_D
350	0.0233	3.7900%	-0.1969	0.001469	36.7314μw
400	0.0267	3.1709%	-0.1969	0.001229	30.7377μw
450	0.0300	0.9149%	-0.1969	0.000354	8.8711μw
500	0.0333	1.1426%	-0.1970	0.000443	11.0817μw
550	0.0367	5.3874%	-0.1970	0.002090	52.2686μw
600	0.0400	7.8545%	-0.1970	0.003049	76.2302μw
650	0.0433	24.3259%	-0.1971	0.009447	236.1782μw
700	0.0467	100.0000%	-0.1971	0.038851	971.2820μw
750	0.0500	7.4633%	-0.1971	0.002900	72.5208μw
800	0.0533	0.8948%	-0.1972	0.000347	8.6985 μw
850	0.0567	0.5028%	-0.1972	0.000195	4.8901 μw
900	0.0600	0.1833%	-0.1973	0.000071	1.7840 μw
950	0.0633	0.0929%	-0.1973	0.000036	0.9041 μw
1000	0.0667	0.1539%	-0.1974	0.000059	1.4994 μw
1050	0.0700	0.0040%	-0.1975	0.000001	0.0387 μw

Based on the previous table, the sensitivity of the photodetector should be greater than or equal 0.0387 μw. If a photodetector does not meet this sensitivity requirement, then technically, the scan system will have to be re-designed for a shorter chirp range. We observe also that this design problem has assumed nonmagnetic interfaces throughout. In the

more realistic scenario, there may well be magnetic materials present in the search, in which case a more general analysis and simulation will have to be carried out based on eqs.(4) and (6).

3. SCHEMATIC SCANNING CONFIGURATION

The scan system is modeled to cover an area of 30 km by 30 km, the dimensions of a mid-size city. Two sectors are created to cover a maximal amount of the area within a unit cell. The first sector is a *horizontal* sector as shown in Fig.3. The sector is created by executing linear scans per line of about 374.15 m, and generating additional scan lines by rotating the Bragg cell, mounted on a stepper motor, in the XZ plane. As the figure shows, such a forward scan leaves a sizable part of the unit cell outside the sector. Following coverage of the first sector, the Bragg cell is rotated by 107^0 (see ref. [Bugoffa thesis] for details), and the second sector is scanned, thereby reducing the unscanned area within the unit cell. The spot sice of the laser beam on the scanned surface is designed to be 1 m, and moves horizontally by 0.5 m steps. In this manner, the unit cell coverage is about 374.15 m × 300 m. Since some of the scanned areas within the two sectors actually overlap, this implies that some of the scanned "objects" may actually be scanned more than once. The scanned area coverage using 2 sectors approaches close to 100%.

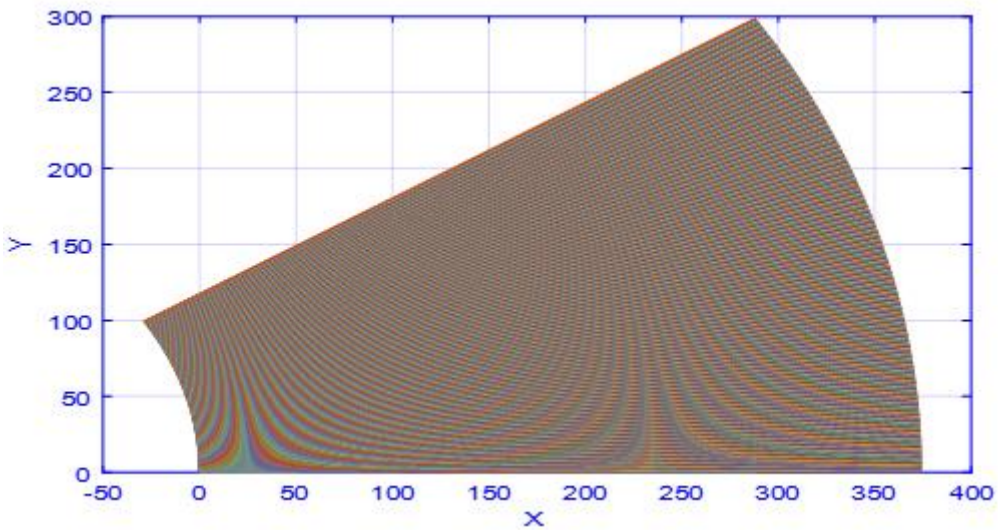

Fig.3. Horizontal sector scan layout in unit cell.

In Fig.3, the sector shown is created in the XY plan by moving the laser spot from the first point (0, 0) by a distance of 0.5 m until the last point at (374.15, 0) is reached, successively changing the incident angle. The return path is a blank; the scan system including the Bragg cell and the laser source mounted on a stepper motor is rotated by a small angle counter clockwise while the RF source is reset to 300 MHz. This process is then continued until the horizontal sector is completed. The uncovered area from the horizontal sector is then covered by a vertical sector created by rotatting the scan system by 107^0 degree counter clockwise. In each return the scan system will rotate a by very small angle clockwise within this time (blank time) as shown; the vertical sector is shown in Fig.4.

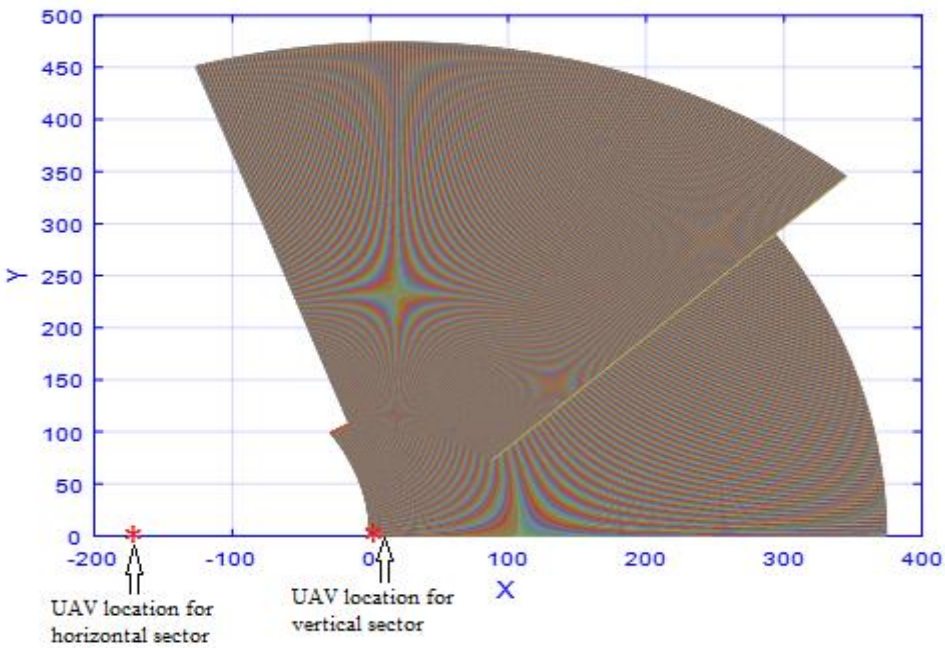

Fig.4. Vertical- and horizontal-sector layout in unit cell.

As can be seen in Fig.4, there is overlapping area between the two sectors. Any object located within the overlapping area will be therefore detected twice and ground control (to which the UAV will transmit sensor coordinates) will receive the coordinates for the detected object twice. The UAV is placed at a height of 8 km above the horizontal plane, and begins the scan process at a location 186.75m behind the "zero" of the scanned unit cell. This distance arises from the minimum incident angle (0.02334 rad). The scanning system requires several time conditions to be prperly met in order to execute the object detection goals set up for this work. Details of all the critical times are discussed further in section 4.

4. NUMERICAL ANALYSIS OF 2-D SCANNING SECTOR

A schematic view of the scanning system and associated components, is shown in Fig.5. The scan system model is designed to achieve the main objective which is to detect all materials on the scanned surface in the horizontal plane with different refractive indices from the seawater (the search area is assumed to be primarily a large body of water, such as the open sea). Note that this scanning model will generally work only for a uniform background over which arbitrary objects are scattered. The Bragg cell is operated via the use of a chirped RF acoustic source with an initial frequency Ω_1 (here taken as 350 MHz) and a center frequency of 700 MHz; it is ensured that the Bragg cell operates in Bragg or near-Bragg conditions throughout the chirp. The first-order scattered beam will initially hit the surface at an angle of 0.02334 rad; the incident scattered beam will subsequently reach the surface to points along the X-axis (for the first scan line) as the chirp frequency changes. All reflected beams (assumed to have Gaussian profiles) will thereafter reach the outer surface of the UAV where a photodetector (PD) will be mounted to intercept the beams. Note that the PD could technically also be mounted inside the UAV- however, this would cause some power loss during propagation through the body of the UAV itself.

In Fig.5, z_{i1} and z_{i2} are the scan ranges for the minimum and maximum scan beams relative to the chirp frequencies. Likewise, z_1 and z_2 are the ranges of the reflected beams in the vertical plane corresponding to the minimum and maximum scan locations. Also, $\theta_{\min}$, $\theta_{\max}$ and θ_B are the Bragg angles corresponding to the minimum, maximum and any intermediate chirp frequency.

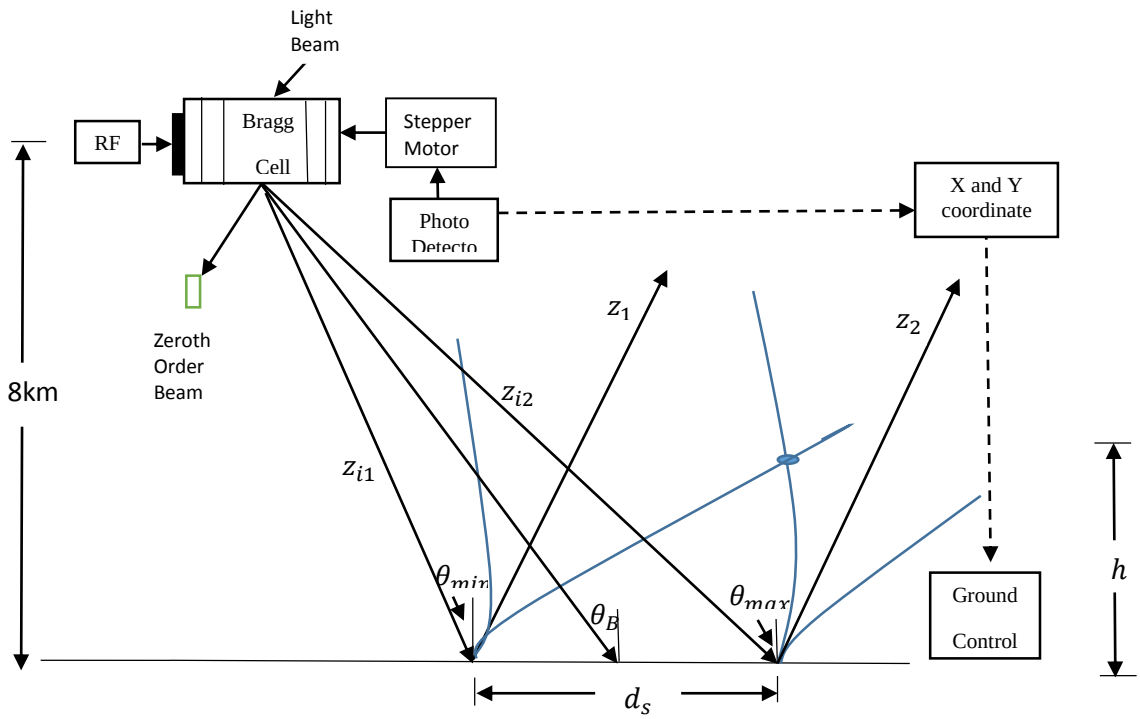

Fig.5. Geometrical layout of the scan system model.

4.1 Optimizing photodetector location

After careful analysis, the optimal placement of the photodetector is found to be on the UAV itself. This determination was made using the following set of equations used to calculate the approximate intersection point between the reflected Gaussian-profile beams from the minimum and maximum angular positions.

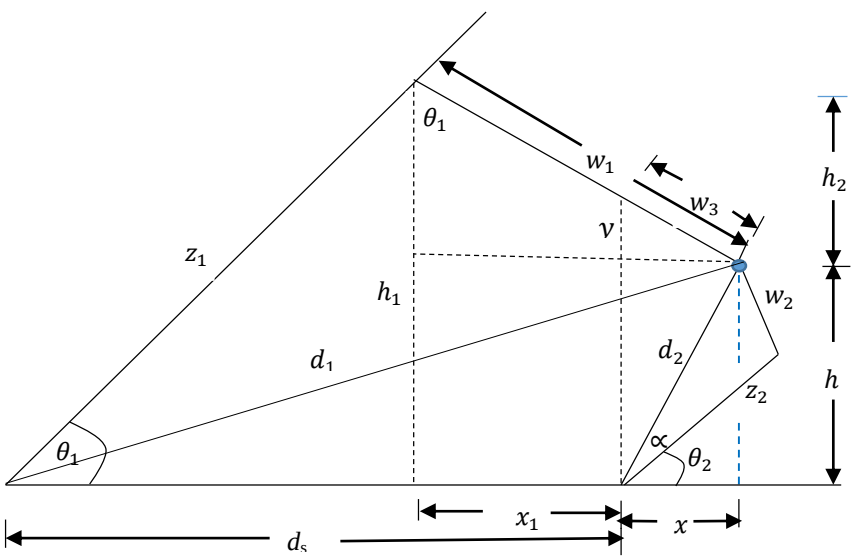

Fig.6. Geometric illustration of the intersection point at height *h* above the horizontal plane.

In Fig.6, z_1 and z_2 represent the physical propagation distance of the reflected Gaussian beams from the minimum and maximum incidence points; w_1 and w_2 are the corresponding beam spot sizes corresponding to the point of intersection of the two Gaussian beams (the right edge of beam 1 and the left edge of beam 2), here linearly connected by d_1 and d_2, as shown. The angles θ_1 and θ_2 are complementary to the minimum and maximum angels of incidence. α represents the divergence angle of the Gaussian beam. h is the vertical height where the two beams intersect, and would represent the minimum altitude where the photodetector would have to be placed in order to intercept the reflected beams across the scan area. From the figure, we find

$$h = d_2 \sin(\theta_2 + \alpha_2) \tag{8}$$

$$d_2 = w_2^2 + z_2^2 \ , \tag{8a}$$

$\theta_1 = 90 - \theta_{min}$, $\theta_2 = 90 - \theta_{max}$ and $\propto =$ diffraction angle of the laser beam.

By solving the above and a set of 9` additional equations (see ref. [8]) simultaneously, the value of h is found to be about 1.5 mm. This negligibly small number implies that *any* detector placed above the horizontal plane should be able to intercept the reflected beams across the entire scanning area. Therefore, placing the photodetector on board the UAV should yield acceptable results.

4.2 Horizontal and vertical linear scanning times (Δt_{ls}) and sector scanning time (Δt_{ss})

The scanning time includes the linear scan time representing the time needed to cover one row with about 694 points, and the full sector scanning consisting of 694 × 600 points. The scan times are calculated numerically assuming a UAV speed of 237 m/s; the results are summarized in Table 2. Note that it is reasonably straightforward to show that the scan times are considerably lower than the propagation time of the UAV across the sectors. Hence the scan operation occurs much faster than it takes for the UAV to enter the scan area. This enables the juxtaposition of horizontal and vertical scans in each unit cell.

Table 2. Scan times.

Horizontal sector		Vertical sector	
Linear scan time	Sector scan time	Linear scan time	Sector scan time
1 μs	0.6 ms	0.3 μs	0.36 ms

Within each sector, the Bragg cell will rotate in a series of steps via the stepper motor; subsequently it must rotate by 107^0 prior to executing the vertical scan. Note that the need to rotate the Bragg cell in the μs time range will require a sufficiently high speed motor- which may require the use of a piezo-motor instead of the stepper motor.

Table 3. Bragg cell rotation angles

Horizontal sector					Vertical sector			
Rotate each step (CCW)	Time	Complete rotation (CW)	Time	One rotate (CCW)	rotate each step (CW)	Time	Complete rotation(CW)	Time
0.051^o	1 μs	30.66^o	0.6 ms	107.1384^o	0.051^o	0.3 μs	63.7577^o	0.36 ms

5. SIMULATION RESULTS AND INTERPRETATIONS

A simulation of the scanning system shown in Fig.5 is implemented in Matlab and the results are presented in this section. The simulation is created based on four randomly distributed materials with different refractive indices in sea water as shown in Fig.7.

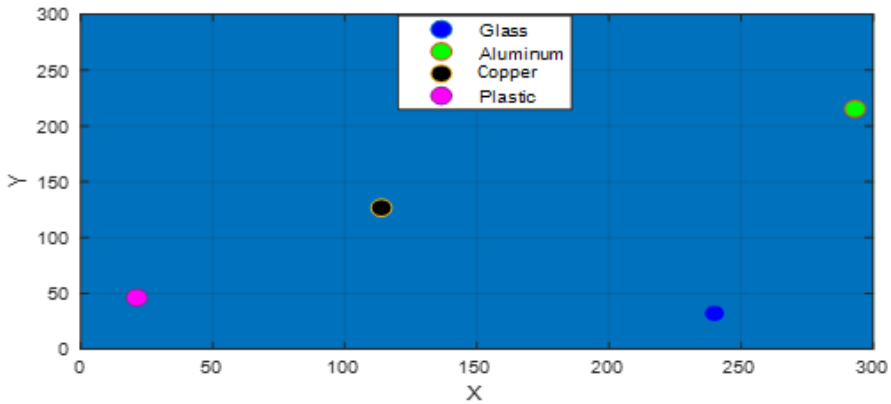

Fig.7. Four randomly distributed materials with different refractive indices.

Fig.8 shows 5 random objects on the scan surface identified by the scan algorithms using the methodology described above. Upon identifying a "hit," the UAV is programmed to transmit to a ground station the coordinates of the scanned "object" following which a ground-based rescue vessel may proceed with retrieval of the "object."

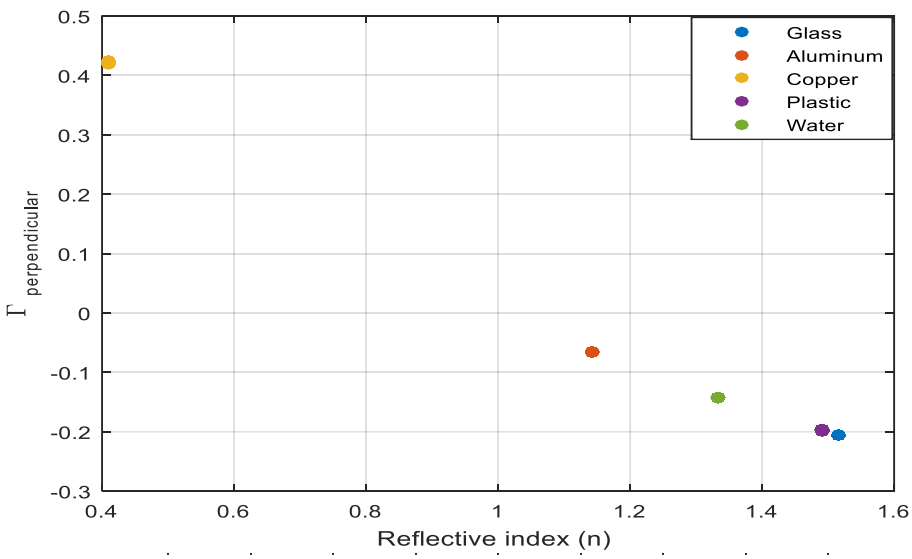

Fig.8. Five distinct materials identified via the scan algorithm showing amplitude reflection coefficient and corresponding refractive indices.

The laser beam reaching the seawater is designed to be 1 m wide; therefore, it is expected to detect objects within a 1m diameter or less, which are typical numbers for a debris field. As discussed, the photodetector mounted outside the UAV will capture the reflections and thereafter send the coordinates (XY) of non-seawater objects to ground control, thereby physically locating the object. If any reflection matches that of seawater reflection, the photodetector will notify a failed scan.

Table 4. Retrieved versus true coordinates for 4 randomly selected objects within the scan area.

Real Coordinate				Scanning Coordinate			
Point 1	Point 2	Point 3	Point 4	Point 1	Point 2	Point 3	Point 4
(240, 32)	(21, 46)	(114, 127)	(293, 215)	(239.8978 32.0071)	(20.9974 45.9130)	(113.9914 126.8031)	(293.0775 215.2245)

As can be seen from Table 4, the error between the actual and scanned coordinates is very small, and this indicates a relatively accurate scan model. Three materials identified by the scan algorithm are shown within the scan area Fig.7.

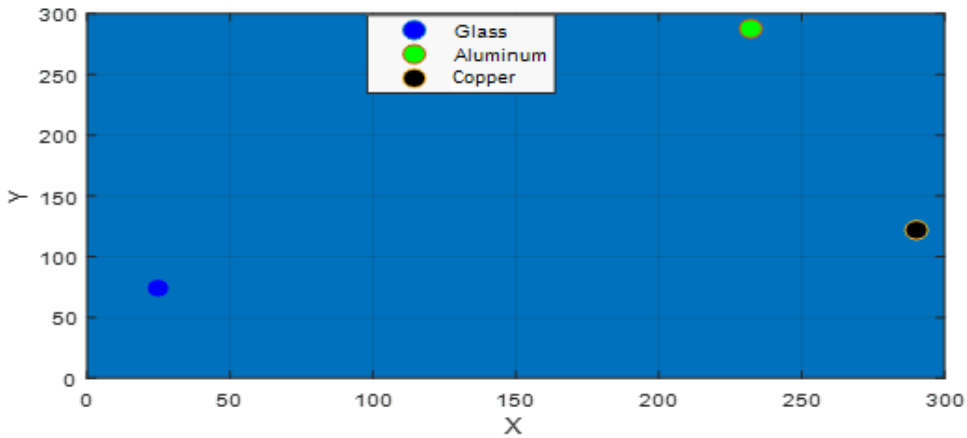

Fig.7. Three random distribution materials with different refractive index

Table 5. Real and retrieved coordinates corresponding to the 3 selected points of Fig.7.

Real Coordinate			Scanning Coordinate		
Point 1	Point 2	Point 3	Point 1	Point 2	Point 3
(290, 122)	(25, 74)	(232, 288)	(289.7715 121.9248)	(24.9694 73.9574)	(231.8006 287.8623)

6. CONCLUDING REMARKS

In this paper, the design and numerical demonstration of a scanning system using a Bragg cell excited by a chirped RF source are presented. Four random materials with different refractive indices are perfectly detected on a seawater background. The optimal Bragg cell length as well as peak phase delay were determined to ensure Bragg operation throughout the chirp range by placing the incident laser beam matched to the center frequency of the chirp (700 MHz). The chirp frequency is designed to be within the range 350 MHz to 1050 MHz; the corresponding Bragg angles are in the mrad range leading to high angular resolution. The scanning systems including the Bragg cell is carried on board a UAV

operating in the XZ plane, and is designed to scan the horizontal surface (XY plane). Vertical and horizontal sectors are created to cover all the scan area. Double (or higher) scanning may occur for any object located within overlapping scan sectors. A photodetector mounted on the outside of the UAV is shown to be active throughout the scanning area. The photodetector is combined with electronics which transmit either a failed scan or the coordinates of any object with refractive index different from seawater reflection to ground control as well as send a signal to the stepper motor to rotate the Bragg cell by pre-selected angles after each line scan. The scanning system is simulated via Matlab and the results indicate high accuracy. The total scan time for covering the designed 30km × 30km scan area is estimated to be about 4.19 hours, which includes the UAV having to make wide 180^0 turns at the end of a complete row scan.

REFERENCES

[1] V.V. Nikulin, R.M. Khandekar and J. Sofka, "Agile acousto-optic tracking system for free space optical communications," Opt. Eng. 47(6), 064301 (2008).

[2] L.H. Gesell, R.E. Feinleib, J.L. Lafuse and T.M. Turpin, "Acousto-optic control of time delays for array beam steering," Proc. SPIE, vol. 2155, pp.194-204, June 1994.

[3] A. Wehr and L. Uwe, "Airborne laser scanning- an introduction and overview," ISPRS J. of Photogram. and Rem. Sensing 54(2), 68-82 (1999).

[4] C.A. Balanis, *Advanced Engineering Electromagnetics*, 2nd Ed., Wiley, NY (2014).

[5] T.-C. Poon and A. Korpel. "Optical transfer function of an acousto-optic heterodyning image processor," Opt. Lett 4(10), 317-391 (1979).

[6] V. Minier, A. Kervorkian, and J.M. Xu, "Diffraction characteristics of superimposed holographic gratings in planar optical waveguides," IEEE Photon. Tech. Lett. 4(10), 1115-1118 (1992).

[7] T.-C. Poon and T. Kim, *Engineering Optics with MATLAB*. World Scientific, Singapore (2006).

[8] S. Bugoffa, MSEE Thesis, University of Dayton, Dayton, Ohio (2016).

[9] S.-T. Chen and M.R. Chatterjee, "A numerical analysis and expository interpretation of the diffraction of light by ultrasonic waves in the Bragg and Raman-Nath regimes using multiple scattering theory," IEEE Trans. Edu. 39(1), 56-68 (1996).

[10] M.R. Chatterjee, T-C. Poon, and D.N. Sitter, Jr., "Transfer function formalism for strong acousto-optic Bragg diffraction of light beams with arbitrary profiles," Acustica 71(2), 81-92 (1990).